Food Sci. Biotechnol. Vol. 14, No. 3, pp. 328 ~ 333 (2005)

Food Science and Biotechnology

Convection Heat Transfer Coefficient of a Meat Cube in a Continuous Flow Sterilizing System

Ji Hyang Hong[1], Young Joe Han[2] and Jong Hoon Chung[3]*

[1]*Research Institute for Agricultural and Life Sciences, Seoul National University, Seoul 151-742, Korea*
[2]*Department of Agricultural and Biological Engineering, Clemson University, Clemson, SC 29634-0312, USA*
[3]*Department of Biosystems & Biomaterials Science and Engineering, Seoul National University, Seoul 151-742, Korea*

Abstract Finite difference model and dynamic thermal property evaluation system were developed to estimate convection heat transfer coefficient by modeling temperature-time profile of beef cube in continuous flow sterilizing system. As input parameters of the model, specific heat and thermal conductivity values of beef frankfurter meat were independently measured from 20 to 80°C. Convection heat transfer coefficient was estimated by comparing simulated and measured temperature-time profiles. Actual temperature-time profiles of meat cube were measured at flow rates of 15, 30, and 45 L/min and viscosities from 0 to 15 cp, and mean values of convection heat transfer coefficients ranged from 792 to 2107 $W/m^2 \cdot K$. Convection heat transfer coefficient increased with increase in flow rate and decreased as viscosity increased.

Keywords: meat cube, frankfurter, aseptic processing, convection, finite difference

Introduction

Aseptic processing is a method for thermal sterile processing of food products, which move in a continuous flow through heat-hold-cool thermal processes and are then packed under sterile conditions. Due to ultra-high temperatures used during the heating process, aseptic processing requires much shorter time as compared to the traditional preparation methods such as retorting. Therefore, it has the potential to minimize damages to food products, improve product quality, reduce energy consumption, and increase productivity. The continuous thermal sterilization process has been favorably used with homogeneous, high-acid foods as an economical and efficient means of destroying microorganisms and inactivating enzymes in foods. However, this process has not been very successful in the case of low-acid foods containing discrete particulate materials due to the problem of assuring complete sterilization.

Sterility of discrete particulate materials can be estimated by measuring the temperature history of the coldest point in a particle moving through a continuous flow thermal process. However no practical method is available to date to measure the temperature of a food particle moving through an aseptic system. In recent years, either biological methods or mathematical models have been used to estimate sterility in low-acid foods containing particulates. Biological methods, although rely on a count-reduction procedure of heat-resistant bacterial spores in inoculated particulates, are tedious and unreliable, because they depend on indefinable conditions of aseptic processing.

Therefore, mathematical simulation models have been popularly applied for predicting the temperature profiles of moving particles to estimate the accumulated lethality during aseptic processing. These models depend on such input parameters as thermal properties of fluids and particulates, convection heat transfer coefficient between fluid and particulate, and residence time in each process. Thermal properties of both particles and fluids such as specific heat and thermal conductivity can be measured experimentally; specific heat of sample foods can be accurately measured using Differential Scanning Calorimetry (DSC) methods (1), and thermal conductivity of both fluids and particulates can be accurately measured using a thermal probe method as reported by Hong *et al.* (2).

However, many mathematical models (3-5) use either infinite or assumed values for convection heat transfer coefficient due to the difficulties of determining reliable values. Because convection heat transfer at the boundary between fluids and particulates can be estimated from temperature-time profiles of fluids and particulates, several apparatuses have been designed to measure the center temperature-time profile of a food particulate in a fluid stream (6-9). Most of these studies mounted a stationary sample in a sample holder and measured the particulate center temperature during continuous flow heating at a constant fluid temperature. However, these studies did not take into consideration the effects of thermal conduction through the sample holding frame and varying characteristics of fluid flow in a real system.

The objectives of the present study were to design a dynamic thermal property evaluation system to measure the temperature-time profiles of a food particulate in aseptic system, develop a finite difference model for the prediction of temperature distribution of a cube particle in aseptic system, estimate the convection heat transfer coefficients from measured and simulated temperature-time profiles of the meat cube, and determine the effects of viscosity and flow rate of the carrier fluid on the convection heat transfer coefficient.

*Corresponding author: Tel: 82-2-880-4601; Fax: 82-2-880-4601
E-mail: jchung@snu.ac.kr
Received April 7, 2005; accepted April 22, 2005

Materials and Methods

Continuous flow sterilizing system An experimental apparatus consisting of a mixing tank, tube-in-shell heat exchanger, pneumatic diaphragm pump, sample-introducing device, sample holder, holding tube, and a custom-made flow meter was developed to simulate a continuous flow sterilizing system (Fig. 1). A 250-L stainless steel mixing tank was thermally insulated with a 5-cm thick glass wool, and a 5.08-cm I.D. drainpipe was attached to the bottom. A custom flow meter, which consisted of a 20-L bucket, baffle tube, fluid level sensors, and a disk valve at the bottom of the bucket, driven by a solenoid on the top of the bucket (Fig. 2), was installed between the third holding-tube section and the mixing tank. A control circuit board and a 1.0-ms clock pulse generator were designed to control the flow rate measurement. Infrared photo devices were installed on the fluid level-indicating tube and used as fluid level sensors. Fluid flow rate was determined by measuring the time required to fill up to 11.3 L volume between the two upper fluid level sensors.

A sample holder was designed to place a sample in the center of the flow tube while minimizing flow disturbance and heat transfer through the sample holder frame (Fig. 3). Brass material was formed into a cross-shaped frame (2.0 ±0.05 mm wide and 3.0±0.05 mm thick) with 13 stainless steel needle tubes (20-gage Type 304 stainless steel #3 temper, Popper and Sons Inc., New Hyde Park, NY, USA) were mounted through the brass frame. Teflon insulated 40-gauge type-T thermocouples (Physitemp Instrument Inc., Clifton, NJ, USA) were installed through the stainless steel needle tubes such that the tip of each thermocouple protruded 7.5 mm from the end of each stainless steel tube. A sample preparation device was designed to make all meat cube samples into exact same size and shape and to form indentations inside the samples for thermocouples. The sample was placed over the thermocouples such that only the ends of the needle tubes were in contact with the surface of the sample to minimize thermal conduction from the frame to the sample. Five thermocouples were placed inside each sample to measure temperatures at the center and four intermediate points. To measure the fluid temperature profiles, eight additional thermocouples were placed around the sample (Fig. 3). All thermocouples were spaced 3.75 mm apart.

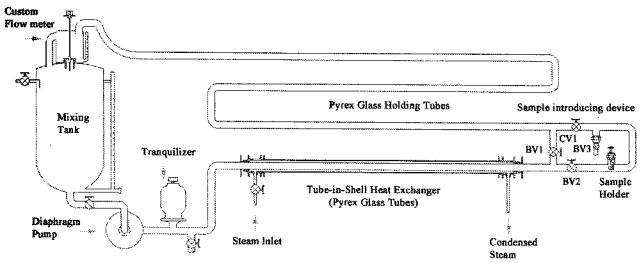

Fig. 1. Schematic diagram of the continuous flow sterilizing system.

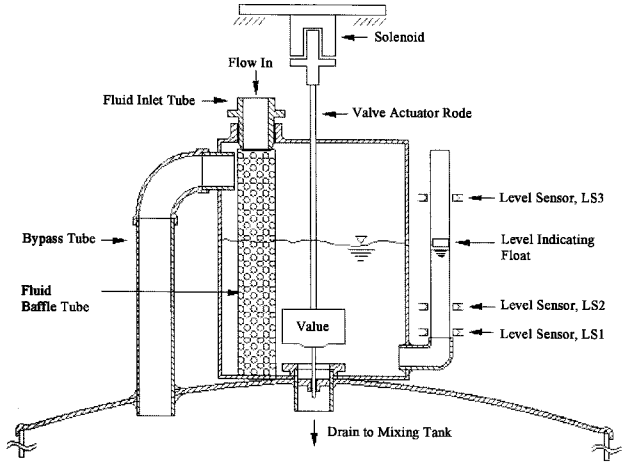

Fig. 2. Schematic diagram of the custom flow meter.

A sample-introducing device was designed to bypass the fluid flow from the sample mounting area, and was placed between the heat exchanger and holding tube section. Figure 4 shows the sample holder mounted in a brass-coupling adapter in a glass T-tube section with a quick coupling device. During the heating of a meat cube in the continuous flow cooking system, the flow pattern was observed through the glass-T where the sample holder was placed. Because the sample was placed in front of the sample holder in the fluid steam (Fig. 4), no pronounced flow disturbance was observed around the sample holder. Temperature profiles inside the sample and fluid around the sample were measured every 2 s with a CR7X measurement and control system (Campbell Scientific, Inc., Logan, UT, USA). The data logger was interfaced to an IBM-PC-compatible microcomputer through an RS-232 port for real-time display and permanent storage of temperature-time profiles and flow rates.

A finite difference model A finite difference model was developed to predict the temperature distributions inside a meat cube in a continuous flow sterilizing system. Because flow patterns at the front, side, and backside of a cube differ with respect to the flow direction, the convection heat transfer rate on each side of the cube will also differ. However, because average value of the heat transfer through all surfaces is the value of interest for engineers in thermal process design, heat transfer rates through all sides of the cube were assumed identical. The model cube was divided into eight identical cubes as mirror images of each other to minimize the computing time. Due to similarities, three-dimensional finite difference equations were derived using energy balances on only four different types of control volumes (inside, side, edge, and corner) (Fig. 5). A mirror image cube was divided into 9x9x9 nodes for a total of 729 nodes with a 0.83-mm nodal spacing.

Finite difference equations can be derived in either explicit or implicit form. For explicit methods, the stability of finite difference equations depends on the Fourier number, Fo:

$$Fo = \frac{k}{\rho C_p (\Delta x)^2} \frac{\Delta \tau}{} \quad (1)$$

Where k, r, C_p, Dt, and Dx denote thermal conductivity, density, specific heat, time step, and nodal size, respectively. For given values of k, r, C_p, and Dx, the stability of finite difference equations can be controlled by

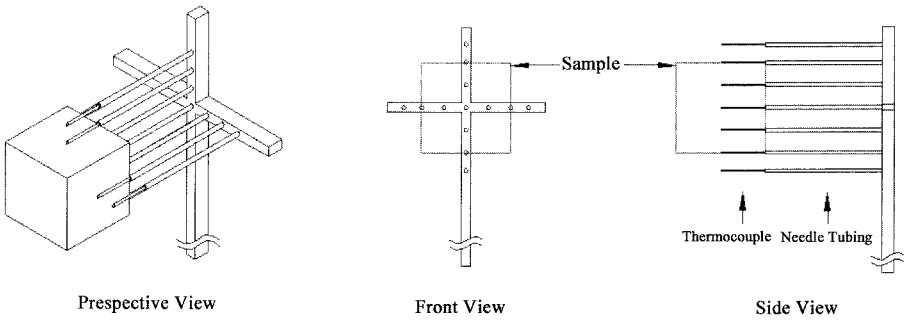

Fig. 3. Schematics of the sample holder and thermocouple locations.

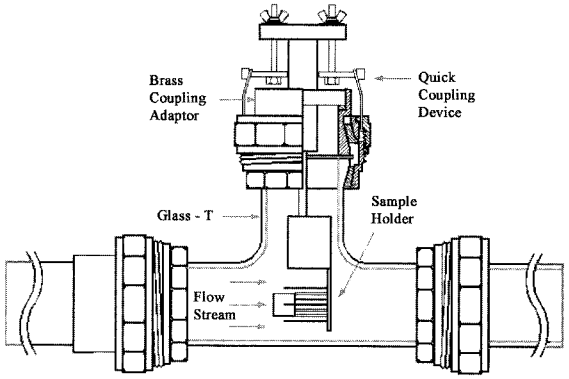

Fig. 4. Schematic of the quick coupling device for the sample holder.

time step size. However, because k and C_p were functions of temperature in this study, it was hard to choose a time step size to assure the stability under all conditions.

Implicit solution methods have an advantage of being stable for any Dt. However, these methods involve large truncation error at every time step, which can be minimized by choosing small Dt. Among implicit solution methods, a Crank-Nicolson method gives the least accumulated truncation error (10). Because the finite difference equations applied in this study used input parameters k and C_p as functions of temperature, the Crank-Nicolson method was employed to develop stable finite difference equations.

For nodes inside a cube, the finite difference equation based on the control volume (Fig. 5a) is:

$$\rho C_p \Delta x\Delta y\Delta z\frac{(T^{p+1}_{l,m,n}-T^{p}_{l,m,n})}{\Delta\tau}=k_{x+}\Delta y\Delta z\frac{(T^{p}_{l+1,m,n}-T^{p}_{l,m,n})}{\Delta x}+k_{x-}\Delta y\Delta z\frac{(T^{p}_{l-1,m,n}-T^{p}_{l,m,n})}{\Delta x}+k_{y+}\Delta z\Delta x\frac{(T^{p}_{l,m+1,n}-T^{p}_{l,m,n})}{\Delta y}+k_{y-}\Delta z\Delta x\frac{(T^{p}_{l,m-1,n}-T^{p}_{l,m,n})}{\Delta z}+k_{z+}\Delta x\Delta y\frac{(T^{p}_{l,m,n-1}-T^{p}_{l,m,n})}{\Delta z} \quad (2)$$

Where ρ, C_p, Δt, $T^{p+1}{}_{l,m,n}$, and $T^{p}{}_{l,m,n}$ denote the density, specific heat, time step, and temperatures at times $p+1$ and p at location (l,m,n), respectively. Based on the equation $\Delta x = \Delta y = \Delta z$ and by setting $\zeta = \rho C_p(\Delta x)^2/\Delta t$, Eq. 2 becomes:

$$\zeta(T^{p+1}_{l,m,n}-T^{p}_{l,m,n})=k_{x+}(T^{p}_{l+1,m,n}-T^{p}_{l,m,n})+k_{x-}(T^{p}_{l-1,m,n}-T^{p}_{l,m,n})+k_{y+}(T^{p}_{l,m+1,n}-T^{p}_{l,m,n})+k_{y-}(T^{p}_{l,m-1,n}-T^{p}_{l,m,n})+k_{z+}(T^{p}_{l,m,n+1}-T^{p}_{l,m,n})+k_{z-}(T^{p}_{l,m,n-1}-T^{p}_{l,m,n}) \quad (3)$$

Using Crank-Nicolson methods, Eq. 3 becomes:

$$\begin{aligned}\zeta(T^{p+1}_{l,m,n}-T^{p}_{l,m,n})=0.5\times[&k_{x+}(T^{p}_{l+1,m,n}-T^{p}_{l,m,n})+k_{x-}(T^{p}_{l-1,m,n}-T^{p}_{l,m,n})\\&+k_{y+}(T^{p}_{l,m+1,n}-T^{p}_{l,m,n})+k_{y-}(T^{p}_{l,m-1,n}-T^{p}_{l,m,n})\\&+k_{z+}(T^{p}_{l,m,n+1}-T^{p}_{l,m,n})+k_{z-}(T^{p}_{l,m,n-1}-T^{p}_{l,m,n})\\&+0.5\times[k_{x+}(T^{p+1}_{l+1,m,n}-T^{p+1}_{l,m,n})+k_{x-}(T^{p+1}_{l-1,m,n}-T^{p+1}_{l,m,n})\\&+k_{y+}(T^{p+1}_{l,m+1,n}-T^{p+1}_{l,m,n})+k_{y-}(T^{p+1}_{l,m-1,n}-T^{p+1}_{l,m,n})\\&+k_{z+}(T^{p+1}_{l,m,n+1}-T^{p+1}_{l,m,n})+k_{z-}(T^{p+1}_{l,m,n-1}-T^{p+1}_{l,m,n})\end{aligned} \quad (4)$$

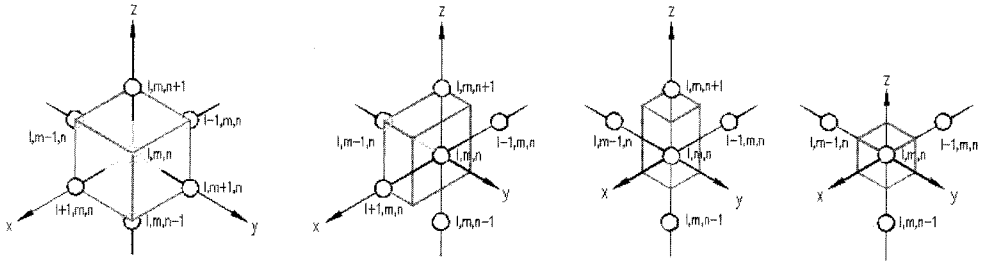

Fig. 5. Control volumes for finite difference equations.

Where ζ was calculated for the C_p value at temperature $T^p_{l,m,n}$ and k_{x+} was the k value for the average temperature of $T_{l+1,m,n}$ and $T_{l,m,n}$. Values of k_x, k_y, and k_z were calculated in a similar way.

For nodes along a side of the model cube, an energy balance based on the control volume (Fig. 5b) is:

$$\begin{aligned}\rho C_p\frac{\Delta x}{2}\Delta y\Delta z\frac{(T^{p+1}_{l,m,n}-T^p_{l,m,n})}{\Delta\tau}&=h\Delta y\Delta z(T^p_f-T^p_{l,m,n})\\&+k_{x-}\Delta y\Delta z\frac{(T^p_{l-1,m,n}-T^p_{l,m,n})}{\Delta x}+k_{y+}\Delta z\frac{\Delta x(T^p_{l,m+1,n}-T^p_{l,m,n})}{\Delta y}\\&+k_{y-}\Delta z\frac{\frac{\Delta x}{2}(T^p_{l,m-1,n}-T^p_{l,m,n})}{\Delta y}+k_{z+}\frac{\Delta x}{2}\Delta y\frac{(T^p_{l,m,n+1}-T^p_{l,m,n})}{\Delta z}\\&+k_{z-}\frac{\Delta x}{2}\Delta y\frac{(T^p_{l,m,n-1}-T^p_{l,m,n})}{\Delta z}\end{aligned}\tag{5}$$

Where h and $T_f{}^p$ denote convection heat transfer coefficient and fluid temperature at time p, respectively. Based on $\Delta x = \Delta y = \Delta z$, and by setting $\zeta = \rho C_p(\Delta x)^2/\Delta\tau$ and $\beta = h\Delta x$, Eq. 5 becomes:

$$\begin{aligned}\zeta(T^{p+1}_{l,m,n}-T^p_{l,m,n})&=2\beta(T^p_f-T^p_{l,m,n})+2k_{x-}(T^p_{l-1,m,n}-T^p_{l,m,n})\\&k_{y+}(T^p_{l,m+1,n}-T^p_{l,m,n})+k_{y-}(T^p_{l,m-1,n}-T^p_{l,m,n})\\&+k_{z+}(T^p_{l,m,n+1}-T^p_{l,m,n})+k_{z-}(T^p_{l,m,n-1}-T^p_{l,m,n})\end{aligned}\tag{6}$$

Using Crank-Nicolson methods, Eq. 6 becomes:

$$\begin{aligned}\zeta(T^{p+1}_{l,m,n}-T^p_{l,m,n})&=0.5\times[2\beta(T^p_f-T^p_{l,m,n})+2k_{x-}(T^p_{l-1,m,n}-T^p_{l,m,n})\\&+k_{y+}(T^p_{l,m+1,n}-T^p_{l,m,n})+k_{y-}(T^p_{l,m-1,n}-T^p_{l,m,n})\\&+k_{z+}(T^p_{l,m,n+1}-T^p_{l,m,n})+k_{z-}(T^p_{l,m,n-1}-T^p_{l,m,n})\\&+0.5\times[2\beta(T^p_f-T^{p+1}_{l,m,n})+2k_{x-}(T^{p+1}_{l-1,m,n}-T^{p+1}_{l,m,n})\\&+k_{y+}(T^{p+1}_{l,m+1,n}-T^{p+1}_{l,m,n})+k_{y-}(T^{p+1}_{l,m-1,n}-T^{p+1}_{l,m,n})\\&+k_{z+}(T^{p+1}_{l,m,n+1}-T^{p+1}_{l,m,n})+k_{z-}(T^{p+1}_{l,m,n-1}-T^{p+1}_{l,m,n})\end{aligned}\tag{7}$$

For nodes at the edge of the model cube, an energy balance based on the control volume (Fig. 5c) is:

$$\begin{aligned}\rho C_p\frac{\Delta x}{2}\frac{\Delta y}{2}\Delta z\frac{(T^{p+1}_{l,m,n}-T^p_{l,m,n})}{\Delta\tau}&=h\frac{\Delta y}{2}\Delta z(T^p_f-T^p_{l,m,n})\\&+k_{x-}\frac{\Delta y}{2}\Delta z\frac{(T^p_{l-1,m,n}-T^p_{l,m,n})}{\Delta x}+h\Delta z\frac{\Delta y}{2}(T^p_f-T^p_{l,m,n})\\&+k_{y-}\Delta z\frac{\frac{\Delta x}{2}(T^p_{l,m-1,n}-T^p_{l,m,n})}{\Delta y}+k_{z+}\frac{\Delta x}{2}\frac{\Delta y}{2}\frac{(T^p_{l,m,n+1}-T^p_{l,m,n})}{\Delta z}\\&+k_{z-}\frac{\Delta x}{2}\frac{\Delta y}{2}\frac{(T^p_{l,m,n-1}-T^p_{l,m,n})}{\Delta z}\end{aligned}\tag{8}$$

Following $\Delta x = \Delta y = \Delta z$, and by setting $\zeta = \rho C_p(\Delta x)^2/\Delta\tau$ and $\beta = h\Delta x$, Eq. 8 becomes:

$$\begin{aligned}\zeta(T^{p+1}_{l,m,n}-T^p_{l,m,n})&=2\beta(T^p_f-T^p_{l,m,n})+2k_{x-}(T^p_{l-1,m,n}-T^p_{l,m,n})\\&+2\beta(T^p_f-T^p_{l,m,n})+2k_{y-}(T^p_{l,m-1,n}-T^p_{l,m,n})\\&+k_{z+}(T^p_{l,m,n+1}-T^p_{l,m,n})+k_{z-}(T^p_{l,m,n-1}-T^p_{l,m,n})\end{aligned}\tag{9}$$

Using Crank-Nicolson methods, Eq. 9 becomes:

$$\begin{aligned}\zeta(T^{p+1}_{l,m,n}-T^p_{l,m,n})&=0.5\times[2\beta(T^p_f-T^p_{l,m,n})+2k_{x-}(T^p_{l-1,m,n}-T^p_{l,m,n})\\&+2\beta(T^p_f-T^p_{l,m,n})+2k_{y-}(T^p_{l,m-1,n}-T^p_{l,m,n})\\&+k_{z+}(T^p_{l,m,n+1}-T^p_{l,m,n})+k_{z-}(T^p_{l,m,n-1}-T^p_{l,m,n})\\&+0.5\times[2\beta(T^p_f-T^{p+1}_{l,m,n})+2k_{x-}(T^{p+1}_{l-1,m,n}-T^{p+1}_{l,m,n})\\&+2\beta(T^p_f-T^{p+1}_{l,m,n})+2k_{y-}(T^{p+1}_{l,m-1,n}-T^{p+1}_{l,m,n})\\&+k_{z+}(T^{p+1}_{l,m,n+1}-T^{p+1}_{l,m,n})+k_{z-}(T^{p+1}_{l,m,n-1}-T^{p+1}_{l,m,n})\end{aligned}\tag{10}$$

For nodes at the corner of the model cube, an energy balance based on the control volume (Fig. 5d) is:

$$\begin{aligned}\rho C_p\frac{\Delta x}{2}\frac{\Delta y}{2}\frac{\Delta z}{2}\frac{(T^{p+1}_{l,m,n}-T^p_{l,m,n})}{\Delta\tau}&=h\frac{\Delta y}{2}\frac{\Delta z}{2}(T^p_f-T^p_{l,m,n})\\&+k_{x-}\frac{\Delta y}{2}\frac{\Delta z}{2}\frac{(T^p_{l-1,m,n}-T^p_{l,m,n})}{\Delta x}+h\frac{\Delta z}{2}\frac{\Delta y}{2}(T^p_f-T^p_{l,m,n})\\&+k_{y-}\frac{\Delta z}{2}\frac{\Delta x}{2}\frac{(T^p_{l,m-1,n}-T^p_{l,m,n})}{\Delta y}+h\frac{\Delta x}{2}\frac{\Delta y}{2}(T^p_f-T^p_{l,m,n})\\&+k_{z-}\frac{\Delta x}{2}\frac{\Delta y}{2}\frac{(T^p_{l,m,n-1}-T^p_{l,m,n})}{\Delta z}\end{aligned}\tag{11}$$

Because $\Delta x = \Delta y = Dz$ and by setting $\zeta = \rho C_p(\Delta x)^2/\Delta t$ and $\beta = h\Delta x$, Eq. 11 becomes:

$$\begin{aligned}\zeta(T^{p+1}_{l,m,n}-T^p_{l,m,n})&=2\beta(T^p_f-T^p_{l,m,n})+2k_{x-}(T^p_{l-1,m,n}-T^p_{l,m,n})\\&+2\beta(T^p_f-T^p_{l,m,n})+2k_{y-}(T^p_{l,m-1,n}-T^p_{l,m,n})\\&+2\beta(T^p_f-T^p_{l,m,n})+2k_{z-}(T^p_{l,m,n-1}-T^p_{l,m,n})\end{aligned}\tag{12}$$

Using Crank-Nicolson method, Eq. 12 becomes:

$$\begin{aligned}\zeta(T^{p+1}_{l,m,n}-T^p_{l,m,n})&=0.5\times[2\beta(T^p_f-T^p_{l,m,n})+2k_{x-}(T^p_{l-1,m,n}-T^p_{l,m,n})\\&+2\beta(T^p_f-T^p_{l,m,n})+2k_{y-}(T^p_{l,m-1,n}-T^p_{l,m,n})\\&+2\beta(T^p_f-T^p_{l,m,n})+2k_{z-}(T^p_{l,m,n-1}-T^p_{l,m,n})\\&+0.5\times[2\beta(T^p_f-T^{p+1}_{l,m,n})+2k_{x-}(T^{p+1}_{l-1,m,n}-T^{p+1}_{l,m,n})\\&+2\beta(T^p_f-T^{p+1}_{l,m,n})+2k_{y-}(T^{p+1}_{l,m-1,n}-T^{p+1}_{l,m,n})\\&+2\beta(T^p_f-T^{p+1}_{l,m,n})+2k_{z-}(T^{p+1}_{l,m,n-1}-T^{p+1}_{l,m,n})]\end{aligned}\tag{13}$$

Finite difference equations (Eq. 4, 7, 10, and 13) were programmed in C++ programming language (Borland International, Inc., City, CA, USA).

Convection heat transfer coefficient To estimate the effects of viscosity and flow rate of the carrier fluid on the convection heat transfer coefficient h_{fp}, temperature-time profiles of six meat cube samples were measured at three levels each of flow rate and fluid viscosity. The effects of flow rate and viscosity levels on h_{fp} were tested using General Linear Model Procedures (GLM) of SAS (11).

Water, and 1 and 2% Carboxymethyl Cellulose Sodium High viscosity(CMC, Sigma Chemical Company, St. Louis, MO, USA) solutions were used as the three viscosity levels, and flow rates were 15, 30, and 45 L/min (Table 1). CMC solutions were prepared by mixing CMC powder with 80°C tap water in the continuous flow cooking system. Viscosity of 1 and 2% CMC solutions, measured at 80°C using a Wells-Brookfield Cone/Plate Viscometer (Brookfield Engineering Lab., Inc., Middleboro, MA, USA) with a 0.8° cone spindle, were 8.4 ± 0.66 and 15.0 ± 0.21 cp, respectively. Carrier fluid temperature at the sample location was maintained 80 ± 1°C during all temperature-time profile measurement cycles.

Thermal properties of intact meat samples depend on the direction of muscle grain to the heat flux. Hill *et al.* (12) found that k values were 8 to 16% higher when measured parallel to the fiber in comparison to those evaluated perpendicular to the muscle fiber grain of beef. To simplify the thermal property determination, a beef frankfurter (Oscar Mayer" brand Beef Franks) was obtained from a local grocery store for testing due to its structural homogeneity. Mean moisture content and density of the beef frankfurters were 53.7 ± 0.44% (wet basis) and 1033 ± 20 kg/m^3, respectively. Moisture content was determined using a convection oven method at 75°C for 24 hr, and density was determined using a graduate cylinder and a balance. Specific heat of the beef meat was measured continuously from 10 to 100°C at 1°C increments using a Differential Scanning Calorimetry (DSC 2920, TA instrument, Co, New Castle, DE, USA). Specific heat of the beef frankfurters ranged between 2729 kJ/kg·K at 20°C and 3567 kJ/kg·K at 42°C. Thermal conductivity of the meat samples was measured using an instrument developed by Hong *et al.* (2) between 20 to 80°C and ranged 0.389 to 0.350 W/m·K.

To estimate h_{fp}, the temperature distribution inside a cube was computed from an initial guess value of h_{fp} until an objective function $J(h_{fp})$ was minimized. $J(h_{fp})$ was defined as the standardized sum of squares of the difference between the calculated center temperature, $T_{cal}(0,0,0,t_n)$, and its corresponding measured center temperature, $T_{exp}(0,0,0,t_n)$:

$$J(h_{fp}) = \frac{1}{N}\sum_{n=1}^{N}[T_{cal}(0,0,0,t_n) - T_{exp}(0,0,0,t_n)]^2 \quad (14)$$

where N denotes the number of data points used in the calculations.

To determine the minimum value of $J(h_{fp})$, an initial value of $J(h_{fp})$ was computed from the initial value of h_{fp}, which was then increased by an initial step size of Δh_{fp}, and a new value of $J(h_{fp})$ was computed for the new h_{fp}. If the value of $J(h_{fp})$ decreased, the value of h_{fp} was again increased by Δh_{fp}. If $J(h_{fp})$ increased, Δh_{fp} was multiplied by -0.5, and the above procedure was repeated until the absolute value of $\Delta J(h_{fp})$ became less than 1.0E-06. The value of h_{fp} that resulted was presented as the estimated convection heat transfer coefficient for the specific experimental setup.

Results and Discussion

A finite difference model Figure 6 shows the measured center temperature-time profile of a meat cube in water, compared with the simulated ones of the cube for h_{fp} values of 200, 400, 600, 1687, and 10000 W/m^2·K. Results showed that fluid temperatures at the sample location reached steady state within 10 s. As the h_{fp} value increased, simulated center temperature profiles approached the measured profile. For h_{fp} values greater than 1687 W/m^2·K, the simulated temperature increased faster than the measured one and best matched with the measured temperatures when h_{fp} value of 1687 W/m^2·K was used, resulting in the minimum $J(h_{fp})$ value in Eq. 14. $J(h_{fp})$ values increased with higher values of h_{fp}, but at a much slower rate, which indicates, as the surface temperature approaches the fluid temperature, the temperature rise at the center points depends more on thermal properties of the solid particulate than the h_{fp} value in this range. Measured and simulated temperature profiles at the middle point between the surface and the center also showed a close match at this minimum $J(h_{fp})$ value (Fig. 7).

Convection heat transfer coefficient Estimated mean h_{fp} values ranged from 792 to 2107 W/m^2·K for beef frankfurter meat cubes over the three levels of flow rate and fluid viscosity (Table 2). Statistical analysis showed

Table 1. Average flow rates of carrier fluids

Carrier Fluid	Flow Rate* ± Standard Deviation (L/min)		
	Low Flow Rate	Medium Flow Rate	High Flow Rate
Water	15.6 ± 0.59	29.7 ± 0.64	45.0 ± 0.63
1%CMC	17.3 ± 0.34	30.3 ± 0.19	44.9 ± 0.12
2%CMC	18.3 ± 0.26	29.2 ± 0.18	45.2 ± 0.26

*Average values of 10 measurements

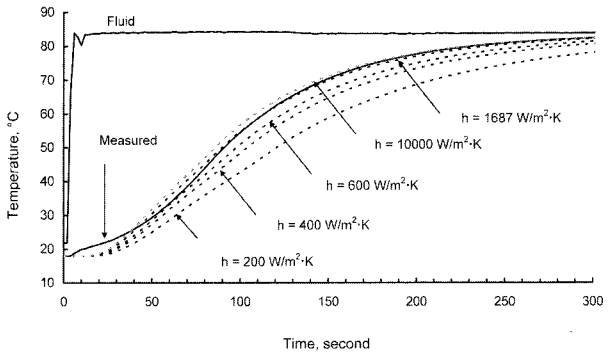

Fig. 6. Simulated and measured center temperature-time profiles of a meat cube in water at a flow rate of 14.5 L/min.

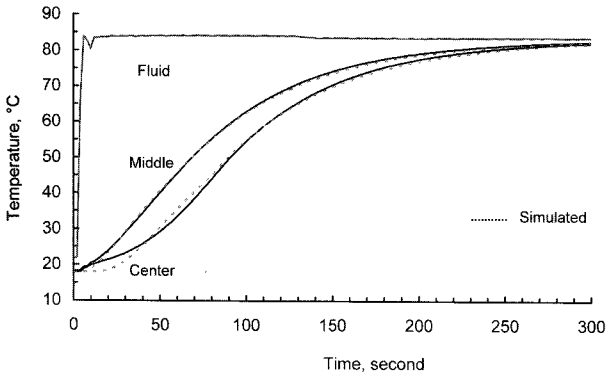

Fig. 7. Simulated and measured temperature-time profiles of the center and middle points of a meat cube for h_{fp} value of 1687 W/m^2·K.

Table 2. Mean convection heat transfer coefficients at various flow rates and in various concentrations of CMC solution

Carrier Fluid	Heat transfer coefficient* ± SD (W/m^2·K)		
	Low Flow Rate	Medium Flow Rate	High Flow Rate
Water	1333 ± 137	2107 ± 691	1704 ± 485
1%CMC	841 ± 111	1131 ± 273	1273 ± 273
2%CMC	792 ± 120	1060 ± 392	1132 ± 220

*Average values of 10 measurements

that convection heat transfer coefficient was significantly influenced by flow rate and viscosity level. Estimated h_{fp} values decreased as viscosity increased, while increased with increasing flow rate in the 1 and 2% CMC solutions. The estimated h_{fp} values in water showed larger variations than those in CMC solutions, probably due to the greater fluctuations in flow rates (Table 1).

To check the dimensional changes of meat cubes during the experimental tests, x, y, and z dimensions of the samples were measured before and after the temperature-time measurement cycle, during which one of the dimensions increased as much as 13%, while the other two decreased up to 5%. Measured temperatures rose faster than the simulated ones for the first 10 s from the start of heating (Fig. 7). Because the shortest path between the surface and the center point determines the heating rate of a meat cube, dimensional changes of meat cubes could have caused the faster rise in the measured temperature. After the first 10 s, the measured temperature profile showed a similar shape to that of the simulated center temperatures, which indicates that no more pronounced dimensional changes occurred after the first 10 s. Due to the dimensional changes, a larger h_{fp} value was required in the finite difference model to make its prediction follow the actual center temperature-time profile. Therefore, h_{fp} values presented in this study could have been overestimated.

References

1. Mohsenin NN. Thermal Properties of Foods and Agricultural Materials. Gordon and Breach Science Publishers, New York, NY, USA (1980)
2. Hong JH, Han YJ, Bunn JM. Measurements of thermal conductivity of food products using a thermal probe method. ASAE Paper No. 98-6001. ASAE, 2950 Niles Rd., St. Joseph, MI, USA (1998)
3. de Ruyter PW, Brunet R. Estimation of process conditions for continuous sterilization of foods containing particles. Food Technol. 27: 44-51 (1973)
4. Manson JE, Cullen JF. Thermal process simulation for aseptic processing of food containing discrete particulate matter. J. Food Sci. 39: 1084-1089 (1974)
5. Sastry SK. Mathematical evaluation of process schedules for aseptic processing of food containing discrete particulate matter. J. Food Sci. 51: 1323-1328 (1986)
6. Alhamdan A, Sastry SK, Blaisdell JL. Natural convection heat transfer between water an irregular shaped particle. Trans. ASAE 33: 620-624 (1990)
7. Chandarana DI, Gavin III A, Wheaton FW. Particle/fluid interface heat transfer during aseptic processing of foods. ASAE Paper No. 88-6599. ASAE, 2950 Niles Rd., St. Joseph, MI, USA (1988)
8. Chang SY. Toledo RT. Heat transfer and simulated steriliza-tion of particulate solids in a continuously flowing system. J. Food Sci. 54: 1017-1023, 1030 (1989)
9. Zuritz CA, McCoy S, Sastry SK. Convective heat transfer coefficients for non-Newtonian flow past food shaped particulates. ASAE Paper No. 87-6538. ASAE, 2950 Niles Rd., St. Joseph, MI, USA (1987)
10. Croft DR, Lilley DG. Heat Transfer Calculations Using Finite Difference equations. Applied Science Publishers, LTD, London, UK pp. 185-187 (1977)
11. SAS Institute Inc. SAS User's Guide. Statistical Analysis System Institute, Cary, NC, USA (1990)
12. Hill JE, Leitman JD, Sunderland JE. Thermal conductivity of various meats. Food Technol. 21: 1143-1148 (1967)